Linear and nonlinear behaviour of near-IR intersubband transitions of cubic GaN/AlN multi quantum well structures

T. Wecker [a,*], T. Jostmeier [b], T. Rieger [c], E. Neumann [c], A. Pawlis [c], M. Betz [b], D. Reuter [a], D.J. As [a,*]

[a] Department of Physics, University of Paderborn, Warburger Str. 100, 33098 Paderborn, Germany
[b] Experimentelle Physik 2, TU Dortmund, 44227 Dortmund, Germany
[c] Peter Grünberg Institut, Forschungszentrum Jülich, 52425 Jülich, Germany

ABSTRACT

The linear and nonlinear behaviour of intersubband transitions of cubic GaN/AlN multi quantum well (QW) structures in the IR spectral region is investigated. In this study photoluminescence, IR absorption as well as pump-probe measurements are done. Two cubic GaN/AlN multi quantum wells with Si content of $N_{Si} \sim 10^{19}$ cm^{-3} in the cubic GaN quantum wells were grown on 3C-SiC (001) substrate by radio-frequency plasma-assisted molecular beam epitaxy. A broad IR absorption with a FWHM of 370 meV was found with a maximum at 0.7 eV, corresponding to the intersubband transition of the multi quantum wells. The nonlinear optical measurement reveals a clear change of transmission for a pump pulse with an angle of incidence of 65°. Furthermore, transmission electron microscopy measurements are used to determine the real layer thicknesses. These thickness values are exploited in the calculation with the Schrödinger-Poisson solver nextnano³. The simulated transition energies agree very well with the experimental data for the photoluminescence and the absorption measurement.

© 2017 Elsevier B.V. All rights reserved.

1. Introduction

Intersubband transitions (ISBT) of multi quantum well (MQW) structures are in the focus of interest for designing several novel devices like quantum cascade lasers, IR detectors and more. Moreover, structures based on the material system of the group III-nitrides have numerous advantages, for instance the high stability against mechanical, thermal, and chemical stress. Therefore structures containing these materials can be investigated using high excitation power, which is favorable for the optical study of nonlinear effects. Especially the ISBT in MQW structures can be exploited to get an insight into nonlinear effects, due to their high nonlinear response. [1–5] In addition, the inherently large band offset between GaN/AlN is beneficial for devices based on ISBT such as THz devices, fast modulators and fast photo detectors [6]. As a result, the ISBT in these devices can reach the 1.55 µm spectral window (optical C-band) [7], suitable for devices in the telecommunication area.

Common hexagonal group III-nitrides suffer from large internal polarization fields along the c-axis resulting in a bending of the bands and the quantum confined Stark-effect. Due to both effects the design of modern devices for intersubband transitions in the

hexagonal phase is reasonably complicated [8]. In order to reduce these effects the growth of hexagonal nitrides in semi-polar directions is intensively investigated [9]. Another approach is the growth of the group III nitrides in the cubic phase in the (001) direction on 3C-SiC. Hence, all above listed unfavorable effects can be significantly reduced [10,11]. Latest results concerning nonlinear optical properties of ISBT for cubic GaN/AlN MQWs can be found in [12].

In this work we study the linear and nonlinear optical behaviour using a photoluminescence, IR absorption as well as a pump-probe setup, respectively. The measured IR absorption shows a broad FWHM of 370 meV and a peak energy of 0.7 eV. The pump-probe measurements provided an angle- and polarization dependent transmission change related to the femtosecond excitation of the ISBT. This is expected for a nonlinear optical response with participation of ISBT transitions in QW structures. The transition energies and the energy levels of the QWs were calculated with the Schrödinger-Poisson solver nextnano³ [13]. Furthermore, transmission electron microscopy (TEM) data were used to compare the expected QW thicknesses with the experimental data, revealing a good agreement.

2. sample description

Two cubic GaN/AlN MQWs were grown on a 100 nm c-GaN buffer layer, which was deposited on a 10 µm 3C-SiC (001) layer on

* Corresponding authors.
 E-mail addresses: wtobias@mail.uni-paderborn.de (T. Wecker), d.as@uni-paderborn.de (D.J. As).

top of a 0.5 mm thick Si substrate. For sample A 80 periods of 1.8 nm thick GaN QWs were grown separated by 1 nm wide AlN barriers (see Fig. 1 left). Sample B contains 20 periods with 1.35 nm GaN QWs and 5 nm AlN barriers (see Fig. 1 right). In both samples the c-GaN QWs were doped with Si in the order of N_{Si} ~10^{19} cm^{-3}. The applied growth system consists of a Riber-32 radio-frequency plasma-assisted molecular beam epitaxy (PAMBE) with standard effusion cells for Ga, Al and Si evaporation. An Oxford plasma source is used as nitrogen source and the growth process is monitored in situ by reflection high energy electron diffraction (RHEED). The growth at a substrate temperature of T_S=720 °C and a nominal excess of one monolayer of Ga at the surface provides the best sample qualities for c-GaN. Deeper insight into the growth of cubic GaN on 3C-SiC can be obtained in Ref. [14].

3. Results

3.1. Structural properties

The structural sample properties were obtained by high resolution X-Ray diffraction (HRXRD) measurements. An average defect density of the order of $D \approx 2 \times 10^{10} cm^{-2}$ was obtained by measuring the width of the rocking curve close to the (002) reflection. Atomic force microscopy measurements revealed a surface roughness of 5–6 nm (rms) for 5×5 µm^2 areas.

Cross-sectional high resolution TEM bright field images (see Fig. 2) of sample B are acquired with a FEI Tecnai G^2 F20 microscope [15]. A TEM lamella was prepared by focused ion beam using Ga ions and a final polishing step with an acceleration voltage of 5 kV. The structural quality is comparable to previous measurements on a similar substrate, which also show an equal interface roughness [16]. For evaluation of the layer thicknesses an intensity profile of the yellow area in Fig. 2 was used. Due to defects and thickness fluctuations, the intensity especially for the thick AlN barriers fluctuates. Thus several line scans in the yellow area are taken to evaluate an average line scan (Fig. 3). Furthermore a mean value for the intensity of the AlN barrier was used (visible as blue lines in Fig. 3.), in order to estimate the layer thicknesses. For the calculation of the thickness the points, at which the intensity between the AlN and GaN layers has dropped to the average value of the materials individual signals, were used (crosses in Fig. 3). This leads to an average width of $(1.2 \pm 0.1) nm$ for the GaN QWs and $(4.77 \pm 0.46) nm$ for the AlN barriers. For the GaN QWs a layer thickness of 1.125 nm (5 ML) and 1.35 nm (6 ML) is expected, due to the monolayer (ML) thickness for c-GaN of 0.225 nm. These two different layer thicknesses lead to the average width of $(1.2 \pm 0.1) nm$ as measured. The best match of the QW layer thickness with the linear optical measurements exploiting nextnano³

Fig. 2. High resolution TEM micrograph of sample B oriented along the <110> direction of the MQWs taken with a FEI Tecnai G^2 F20 microscope.

Fig. 3. TEM intensity contrast profile averaged over the yellow area in Fig. 2 (Sample B). The average QW thickness is $(1.2 \pm 0.1) nm$ and the average thickness for the AlN barriers is $(4.77 \pm 0.46) nm$.

is 1.35 nm. Although these TEM measurements are taken for a different sample, they can be used to calibrate the nextnano³ transition energies.

3.2. Linear optical measurements

Photoluminescence (PL) measurements were conducted with a Nd: YAG laser emitting at 266 nm and a CCD array (Andor iDus 420). Fig. 4 depicts the room temperature interband PL spectrum of sample A in a semi-logarithmic scale. Two emission bands at 3.20 eV and 3.526 eV are visible. These emission bands could be assigned to the c-GaN buffer and the MQWs, respectively. Based on nextnano³ calculations, emission from the MQWs at 3.65 eV for 1.8 nm well width and at 3.6 eV for 2.025 nm well width is expected. But to compare these energies with the PL emission, the exciton binding energy has to be considered. This binding energy is in QWs increased due to the confinement to 52 meV for 1.8 nm and 51 meV for 2.025 nm thick QWs [17]. The red line in Fig. 4 correspond to the corrected energy transition for a 2.025 nm thick QW, which is close to the experimental emission. Apparently the nominally 1.8 nm thick QWs are one monolayer thicker than intended.
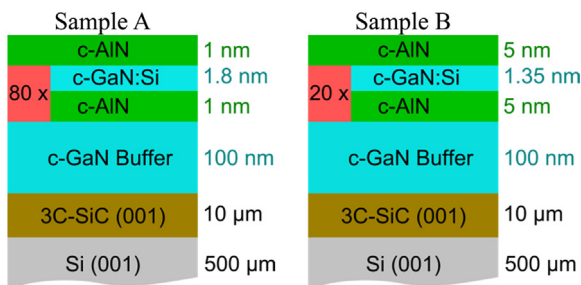

Fig. 1. Sample structure of two MQW samples. Sample A (left) has 80 periods of 1.8 nm GaN QWs and 1 nm AlN barriers. Sample B (right) contains 20 periods of 1.35 nm GaN QWs and 5 nm AlN barriers. Both samples have a Si doping in the c-GaN QWs in the order of N_{Si} ~ 10^{19} cm^{-3}.

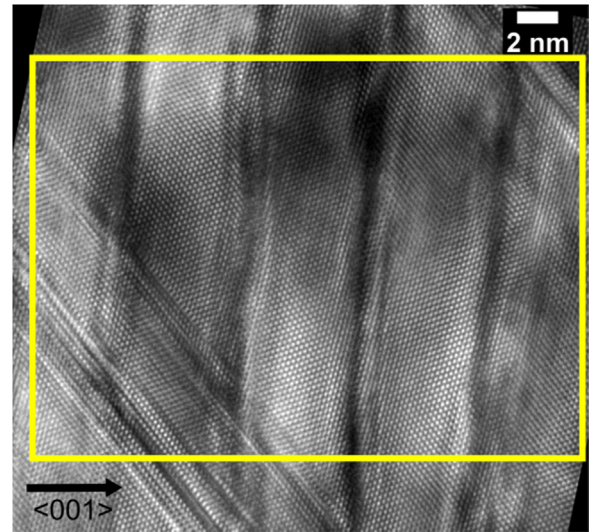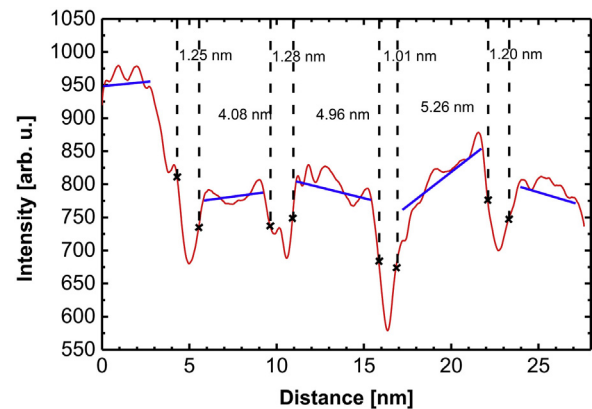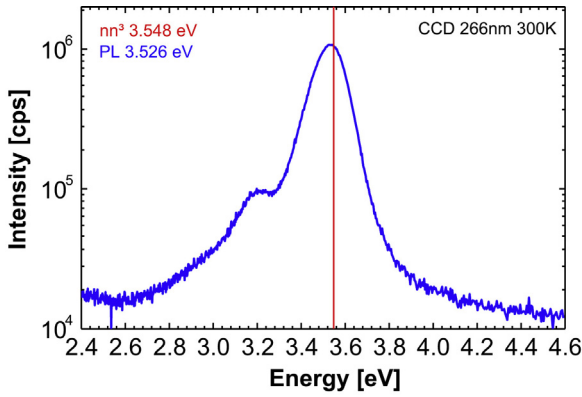**Fig. 4.** Semi-logarithmic plot of the room temperature PL spectrum of sample A. The two emission bands correspond to the c-GaN buffer and the MQWs. The red line indicates the predicted transition energy of the MQWs calculated by nextnano³ corrected by the expected exciton binding energy.

The absorption measurements of the ISBT for sample A are taken with a tungsten light source and a monochromator equipped with an InGaAs photodiode. Due to the transition matrix element for ISBT, the incident light must have a component of the electric field along the growth axis. As a result, we choose a geometry far off normal incidence. To this end, a waveguide is formed with side facets polished under an angle of 30°. This way, we achieve ~20 passes through the MQW structure, cf. inset in Fig. 5. Although the tilted side facets change the angle of incidence of the excitation light with respect to the MQWs, it is a compromise to increase the absorption. The incident light arrive perpendicular to the surface of the 30° facet (cf. inset in Fig. 5). In addition, due to the selection rules for ISBTs the absorption is only expected for TM polarized excitation. In order to obtain the absorption spectrum the detected spectra for TM and TE excitation are subtracted for the MQW sample. Moreover, a reference sample of 600 nm c-GaN with equivalent 30° facets was used to identify spectral features of the substrate and the c-GaN buffer layer contained in the absorption data. The spectrum in Fig. 5 is achieved subtracting the different TM and TE transmissions through the waveguide structure and normalize this by the spectrum of the reference. The red curve indicates a fit curve, as a guide for the eye and for determining the maximum. This spectrum contains additional oscillations, which are related to Fabry-Perot fringes caused by the 10 μm thick
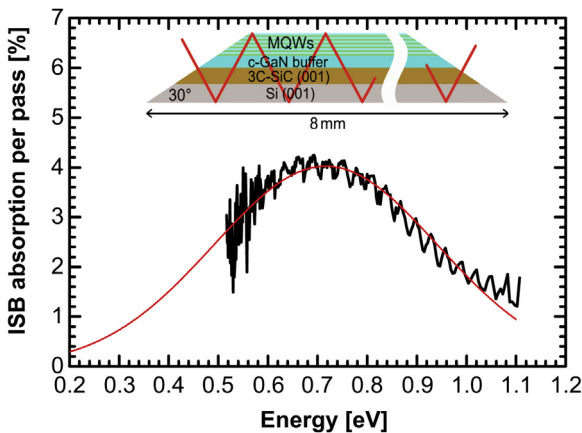
3C-SiC layer. All absorption measurements were performed at room temperature. The absorption maximum at 0.7 eV fits to the calculated value of 0.73 eV, with only a small deviation of 30 meV. The FWHM of this absorption spectrum is 370 meV. This FWHM is higher than that cited in literature for both the cubic [18,6] and the hexagonal [19–21] phase. We think that the strong coupling of the MQWs through the thin AlN barriers may be the reason for this broadening. Moreover the TEM measurements for sample B (Fig. 2, Fig. 3) indicate a fluctuation of the QW thickness, which is also expected for sample A. This further broadens the absorption.

3.3. Nonlinear optical measurements

A degenerate femtosecond pump-probe setup was used to investigate the ultrafast and nonlinear dynamical response of the ISBT of sample A. This setup contains an optical parametric amplifier (Coherent OPA 9850) emitting 50 fs pulses at 250 kHz repetition rate. The central wavelength is tuneable from 0.8 to 0.9 eV, which is close to the ISBT maximum. For this measurement within the ISBT resonance the waveguide structure shown in the inset of Fig. 5 cannot be used. Instead of that only a single pass of the excitation and probe light far off normal incidence is used. Previous investigation of the nonlinear behaviour indicated strong influence of the Si substrate layer, related to two-photon absorption in bulk Si. To eliminate this influence the sample was glued onto a fused silica window and the backside Si was removed mechanically. As a reference, a SiC/Si sample without any MBE grown layer was processed in the same fashion to identify additional features caused by SiC or SiO₂. The results can be seen in Fig. 6. The blue curve belongs to the TE polarized excitation with 65° angle of incidence, where no nonlinear effect is measured as expected. This angle is close to the Brewster angle leading to a better transmission for TM polarized light. Besides the black and the red curve correspond to the TM polarized light with 0° and 65° angle of incidence as indicated in the inset. For the angle of 90° normally no coupling is expected, but the roughness of the interfaces allow for some intensity at this angle. The coupling between the light and some residual in-plane components of the electric field in the ISBT is for 65° higher than for 90°, because the component parallel to the MQW layers is increased. The pump pulse excites charge carriers into higher energy levels, such that the absorption of the probe light is reduced. Additional measurements with variation of the pump irradiance revealed a third order susceptibility in the order of $Im\chi^{(3)} \sim 1.1 \cdot 10^{-20} m^2/V^2$ as described in [12].
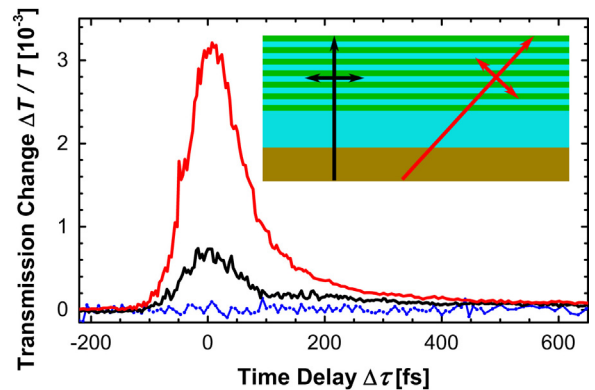

Fig. 5. IR absorption spectrum of the ISBT of sample A at room temperature. The FWHM is 370 meV and the maximum is at 0.7 eV. The inset shows the sample geometry used for the measurement. The red curve corresponds to a fit function as a guide for the eye.

Fig. 6. Pump induced change of the transmission of the MQW for a central photon energy of 0.82 eV. The blue curve corresponds to TE polarized light (angle of incidence 65°). The black and red curves belong to the TM polarization with different angle of incidences, as can be seen in the inset.
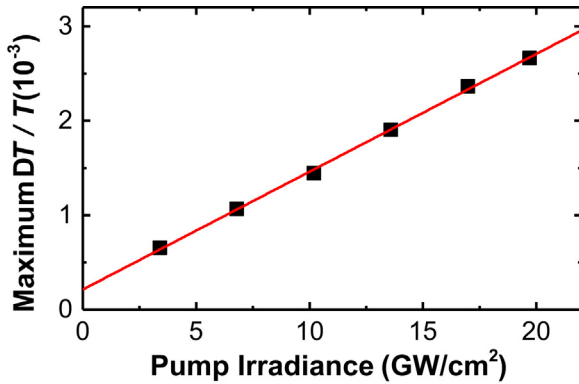
Fig. 7. The peak pump-probe signal for various pump irradiances (central photon energy 0.81 eV, TM polarization, 65° angle of incidence). The red line is a linear fit.
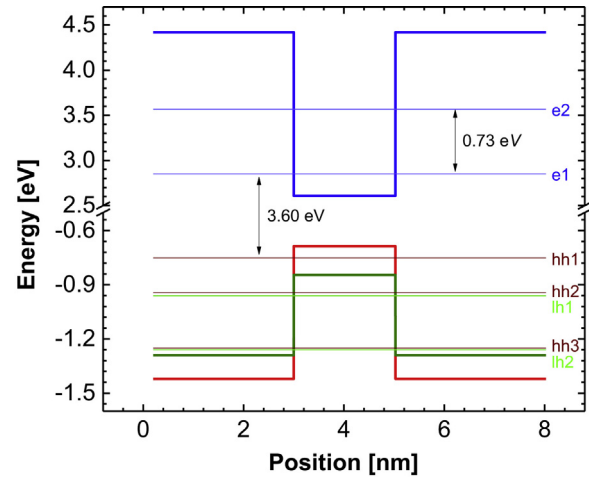

Fig. 8. Band diagram of sample A (d_{QW}=2.025 nm) at room temperature. Due to partly strain in the AlN and GaN layers there is no degeneration of the hh and lh valence bands. The degree of relaxation used for calculations is 0.5.

Fig. 7 depicts the maximum transmission change at nominally zero time delay for different irradiance of pump pulses with 0.81 eV central photon energy. The linear behaviour indicates, that the absorption of the pump pulse doesn't saturate. For the nonlinear optical susceptibilities, this finding suggests that the pump probe measurements are restricted to the $\chi^{(3)}$ regime. The pump power has no significant influence on the temporal shape of the transients.

3.4. Nextnano³ simulations

Simulations of the band structure are performed in order to obtain a detailed understanding of the experimental data. A Schrödinger-Poisson solver (nextnano³ [13]) is used to determine the energy levels of the structure as well as the allowed transitions. Calculations with nextnano³ are based on an effective mass model. For the ration of conduction and valence band offsets between GaN and AlN a value of 74:26 was assumed [22]. Taking into account the mechanical strain within the QW structure X-ray measurements show that the degree of relaxation is about 0.5. For such a degree of relaxation in the QWs inter- and intraband transition energies are calculated as given in Table 1. In the nextnano³ calculations no excitonic effects are considered. The exciton binding energies are calculated separately and are subsequently taken into account, when comparing with PL data [17]. Details for the simulations parameters and the exciton treatment can be found in [23].

Fig. 8 shows the band diagram of sample A for a QW thickness of 2.025 nm with the different energy levels at room temperature. Due to the partly strained AlN barriers the QW is also strained. This results in an average lattice constant of the MQW structure. In nextnano³ only pseudomorphical strained or unstrained layers can be calculated. So the lattice constant of the cubic GaN buffer layer is adapted to realize a partial strain of the MQW structure [23]. The transition responsible in photoluminescence is the first heavy hole to the first electron transition (e1-hh1). For the IR absorption measurements the first and the second electron levels take part (e1-e2).

4. Conclusions

The intersubband transitions of cubic GaN/AlN multi quantum well (MQW) structures are investigated. For the optical characterization photoluminescence (PL), IR absorption and pump-probe measurements are used. The PL revealed two emission bands for the c-GaN buffer layer and the MQW structure. The IR absorption data show a broad absorption with a FWHM of 370 meV centered at 0.7 eV. Nonlinear behaviour was found with a pump-probe setup, leading to a clear transmission change for a pump pulse with an angle of incidence of 65° in case of TM polarized excitation. Furthermore, TEM data show a fluctuation of the layer thicknesses, with a width of 1.35 nm for the GaN QWs. This value was applied into the simulation with nextnano³, revealing a good match of the linear optical transitions and the theory.

Table 1

Inter- and intraband transition energies calculated with nextnano³ for cubic AlN/GaN quantum wells with different well widths. The degree of relaxation was assumed to be 0.5 and no excitonic binding energy was taken into account.

	Sample A	Sample B
Width (nm)	2.025	1.35 nm
e1-hh1 (eV)	3.60	3.82
e1-e2 (eV)	0.73	1.14

References

[1] N. Suzuki, N. Iizuka, Jpn. J. Appl. Phys. 37 (1998) 369.
[2] C. Gmachl, S.V. Frolov, H.M. Ng, S.N.G. Chu, A.Y. Cho, Electron. Lett. 37 (2001) 178.
[3] J.D. Heber, C. Gmachl, H.M. Ng, A.Y. Cho, Appl. Phys. Lett. 81 (2002) 1237.
[4] N. Iizuka, K. Kaneko, N. Suzuki, Electron. Lett. 40 (2004) 962.
[5] J. Hamazaki, S. Matsui, H. Kunugita, K. Ema, H. Kanazawa, T. Tachibana, A. Kikuchi, K. Kishino, Appl. Phys. Lett. 84 (2004) 1102.
[6] H. Machhadani, M. Tchernycheva, L. Rigutti, S. Saki, R. Colombelli, C. Mietze, D. J. As, F.H. Julien, Phys. Rev. B 83 (2011) 075313.
[7] C. Gmachl, H.M. Ng, Electron. Lett. 39 (2003) 567.
[8] M. Beeler, C. Bougerol, E. Bellet-Amalaric, E. Monroy, Phys. Status Solidi (a) 211 (4) (2014) 761–764.
[9] F. Scholz, Semicond. Sci. Technol. 27 (2012) 024002.
[10] D.J. As, C. Mietze, Phys. Status Solidi (a) 210 (2013) 474.
[11] C. Mietze, M. Bürger, S. Sakr, M. Thernycheva, F.H. Julien, D.J. As, Phys. Status Solidi (a) 210 (2013) 455.
[12] T. Jostmeier, T. Wecker, D. Reuter, D.J. As, M. Betz, Appl. Phys. Lett. 107 (2015) 211101.
[13] S. Birner, S. Hackenbuchner, M. Sabathil, G. Zandler, J.A. Majewski, T. Andlauer, T. Zibold, R. Morschl, A. Trellakis, P. Vogl, Acta Phys. Pol. A 110 (2006) 111.
[14] J. Schörmann, S. Potthast, D.J. As, K. Lischka, Appl. Phys. Lett. 90 (2007) 041918.

[15] M. Luysberg, M. Heggen, K. Tillmann, JLSRF 2 (2016) 138.
[16] R.M. Kemper, P. Veit, C. Mietze, A. Dempewolf, T. Wecker, F. Bertram, J. Christen, J.K.N. Lindner, D.J. As, Phys. Status Solidi (C.) 12 (2015) 469.
[17] H. Mathieu, P. Lefebvre, P. Christol, Phys. Rev. B 46 (1992) 4093.
[18] E.A. DeCuir, E. Fred, M.O. Manasreh, J. Schörmann, D.J. As, K. Lischka, Appl. Phys. Lett. 91 (2007) 041991.
[19] A. Helman, M. Tchernycheva, A. Lusson, E. Warde, F.H. Julien, Kh Moumanis, G. Fishman, E. Monroy, B. Daudin, D. Le Si Dang, E. Bellet-Amalric, D. Jalabert, Appl. Phys. Lett. 83 (2003) 5196.
[20] M. Tchernycheva, L. Nevou, L. Doyennette, F.H. Julien, E. Warde, F. Guillot, E. Monroy, E. Bellet-Amalric, T. Remmele, M. Albrecht, Phys. Rev. B 73 (2006) 125347.
[21] X.Y. Liu, P. Holmstrm, P. Jnes, L. Thyln, T.G. Andersson, Phys. Status Solidi (a) 244 (2007) 2892.
[22] C. Mietze, M. Landmann, E. Rauls, H. Machhadani, S. Sakr, M. Tchernycheva, F. H. Julien, W.G. Schmidt, K. Lischka, D.J. As, Phys. Rev. B 83 (2011) 195301.
[23] T. Wecker, G. Callsen, A. Hoffmann, D. Reuter, D.J. As (05FG01) Jpn. J. Appl. Phys. 55 (2016) (05FG01).